Letter

Origin of transverse voltages generated by thermal gradients and electric fields in ferrimagnetic-insulator/heavy-metal bilayers

Arnab Bose [1,2,*], Rakshit Jain,[2,*] Jackson J. Bauer [3], Robert A. Buhrman,[1] Caroline A. Ross,[3] and Daniel C. Ralph[2,4]

[1]*School of Applied and Engineering Physics, Cornell University, Ithaca, New York 14853, USA*
[2]*Department of Physics, Cornell University, Ithaca, New York 14853, USA*
[3]*Department of Materials Science and Engineering, Massachusetts Institute of Technology, Massachusetts 02139, USA*
[4]*Kavli Institute at Cornell for Nanoscale Science, Ithaca, New York 14853, USA*

We compare thermal-gradient-driven transverse voltages in ferrimagnetic-insulator/heavy-metal bilayers ($Tm_3Fe_5O_{12}$/W and $Tm_3Fe_5O_{12}$/Pt) to corresponding electrically driven transverse resistances at and above room temperature. We find for $Tm_3Fe_5O_{12}$/W that the thermal and electrical effects can be explained by a common spin-current detection mechanism, the physics underlying spin Hall magnetoresistance (SMR). However, for $Tm_3Fe_5O_{12}$/Pt the ratio of the electrically driven transverse voltages (planar Hall signal/anomalous Hall signal) is much larger than the ratio of corresponding thermal-gradient signals, a result which is very different from expectations for a SMR-based mechanism alone. We ascribe this difference to a proximity-induced magnetic layer at the $Tm_3Fe_5O_{12}$/Pt interface.

I. Introduction. In solid-state materials that have a magnetic moment or are subject to an external magnetic field (H_{ext}), an applied electric field (E) or thermal gradient (∇T) can generate transverse charge currents and voltages, resulting in Hall effects, anomalous Hall effects [1], or Nernst effects [2]. In systems with strong spin-orbit coupling, an E or ∇T can also drive analogous transverse-flowing spin currents, yielding spin Hall effects (SHE) [3] or spin Nernst effects [4]. When heterostructures are made containing both layers with strong spin-orbit coupling and magnetic layers, spin currents can themselves generate transverse voltages and novel forms of magnetoresistance. The precise mechanisms by which these spin-current-driven electrical signals arise has been a matter of controversy, with arguments made for combinations of spin Hall magnetoresistance (SMR) [5,6] magnetic proximity effects (MPE) [7,8], and magnetic scattering [9]. Here we investigate these issues using a simple model system—combining a thin film of heavy metal with an insulating ferrimagnet ($Tm_3Fe_5O_{12}$ = TmIG), so that the transport characteristics are not affected by charge flow within the magnetic layer. We compare thermally driven transverse voltages to their electrically driven counterparts. We find that different mechanisms are active between TmIG/W and TmIG/Pt. In TmIG/W, both electrically driven and thermally driven transverse voltages can be understood from a single spin-current detection mechanism, the physics that gives rise to SMR. In TmIG/Pt, this is not the case, and we conclude that a MPE in the Pt as well as SMR affect the results.

II. Backround: Spin Hall and anisotropic magnetoresistance. When E is applied to generate a charge current density J_C within the plane of a ferrimagnetic insulator/ heavy metal

(HM) bilayer, a spin current density $J_S = \theta_{SH}(J_C \times \sigma)$ is created due to the SHE in the HM [Fig. 1(a)] with θ_{SH} as the spin Hall ratio of the HM and σ as the orientation of the current-generated spins being in-plane and perpendicular to J_C. A fraction of J_S can be reflected at the interface depending upon the angle between σ and the magnetization M. The reflected spin current is then transduced back into an electric voltage within the HM by the inverse SHE. For the definition of coordinate axes shown in Fig. 1(b), the resulting spin Hall magnetoresistance produces changes in the longitudinal (ρ_{xx}) and transverse (ρ_{xy}) resistivity,

$$\rho_{xx} = \rho_0 + \Delta\rho_{xy}^{\phi,SMR} m_y^2 \qquad (1)$$

$$\rho_{xy} = \Delta\rho_{xy}^{z,SMR} m_z + \Delta\rho_{xy}^{\phi,SMR} m_x m_y \qquad (2)$$

where $m_x = \sin\theta \cos\phi$, $m_y = \sin\theta \cos\phi$, and $m_z = \cos\theta$ represent the orientation of the magnetization saturated parallel to the applied magnetic field and $\Delta\rho_{xy}^{\phi,SMR}$ and $\Delta\rho_{xy}^{z,SMR}$ are the SMR coefficients. The values of $\Delta\rho_{xy}^{\phi,SMR}$ and $\Delta\rho_{xy}^{z,SMR}$ are predicted to depend on the real and imaginary parts of the effective spin mixing conductance of the interface ($G_{eff}^{\uparrow\downarrow}$) [6,10],

$$\frac{\Delta\rho_{xy}^{\phi,SMR}}{\rho_0} = \theta_{SH}^2 \frac{\lambda}{t_{HM}} 2\lambda\rho_0 \text{Re}\left(G_{eff}^{\uparrow\downarrow}\right), \qquad (3)$$

$$\frac{\Delta\rho_{xy}^{z,SMR}}{\rho_0} = -\theta_{SH}^2 \frac{\lambda}{t_{HM}} 2\lambda\rho_0 \text{Im}\left(G_{eff}^{\uparrow\downarrow}\right), \qquad (4)$$

where for the heavy metal λ is the spin-diffusion length, and t_{HM} is the thickness, and $G_{eff}^{\uparrow\downarrow} = G^{\uparrow\downarrow}\tanh^2\frac{t_{HM}}{2\lambda}/[1 + 2\lambda\rho_0 G^{\uparrow\downarrow} \coth\frac{t_{HM}}{\lambda}]$ where $G^{\uparrow\downarrow}$ is the bare interfacial spin mixing conductance.
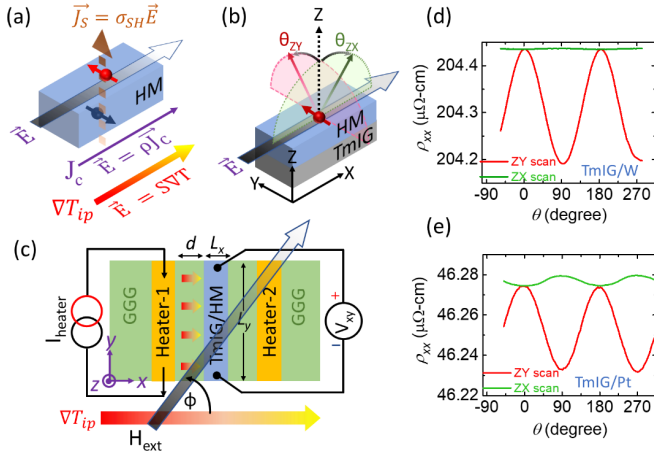
*The authors contributed equally to this work.

FIG. 1. (a) Origin of spin current generation by the spin Nernst effect. (b) Orientation of magnetic-field rotation for z-y and z-x scans. (c) Schematic of the experimental setup for measurement of transverse voltages generated by a ∇T. (d) and (e) ρ_{xx} of the heavy metal layer for (d) TmIG/W and (e) TmIG/Pt.

The existence of a spin Nernst effect in ferromagnet/HM bilayers, a thermal analog to the SHE, has been reported in Refs. [11–16]. In this case, an in-plane thermal gradient (∇T_{ip}) in a sample with no net charge current flow (i.e., open-circuit condition) generates a spin current density,

$$J_S = -\theta_{SN}\frac{S_{HM}}{\rho_{HM}}(\nabla T_{ip} \times \sigma) \quad (5)$$

where θ_{SN} is the spin Nernst angle and S_{HM} is the Seebeck coefficient of the HM. One can alternatively define a different quantity (we will call this θ_{SN}^0) to characterize the spin current generated by ∇T_{ip} in a sample with no longitudinal electric field so that in the presence of an electric field the total transverse spin current has the form

$$J_S = \theta_{SH}\frac{1}{\rho_{HM}}(E \times \sigma) - \theta_{SN}^0\frac{S_{HM}}{\rho_{HM}}(\nabla T_{ip} \times \sigma). \quad (6)$$

In the open-circuit condition corresponding to our measurements, there is a longitudinal electric field due to the Seebeck effect, $E = S_{HM}\nabla T_{ip}$, so that

$$\theta_{SN} = -\theta_{SH} + \theta_{SN}^0. \quad (7)$$

A thermally generated J_S reflected at the interface can again be transduced into a voltage by the inverse SHE in the HM, resulting in thermally induced voltages in both the longitudinal and the transverse directions [11–13],

$$\frac{V_{xx}^{T-SMR}}{L_x} = -\left(S_{HM} + \Delta S_0^{SMR} + \Delta S_{xy}^{\phi,SMR}m_y^2\right)\nabla T_{ip}, \quad (8)$$

$$\frac{V_{xy}^{T-SMR}}{L_y} = -\left(\Delta S_{xy}^{zSMR}m_z + \Delta S_{xy}^{\phi,SMR}m_xm_y\right)\nabla T_{ip}, \quad (9)$$

where L_x and L_y are the length and width of the device [Fig. 1(c)]. Within the framework of the SMR spin-current detection mechanism, one would expect [10]

$$\frac{\Delta S_{xy}^{\phi,SMR}}{S_{HM}} = \theta_{SH}\theta_{SN}\frac{\lambda}{t_{HM}}2\lambda\rho_0\mathrm{Re}\left(G_{eff}^{\uparrow\downarrow}\right), \quad (10)$$

$$\frac{\Delta S_{xy}^{z,SMR}}{S_{HM}} = -\theta_{SH}\theta_{SN}\frac{\lambda}{t_{HM}}2\lambda\rho_0\mathrm{Im}\left(G_{eff}^{\uparrow\downarrow}\right) \quad (11)$$

If SMR is the only mechanism contributing to both the electrically driven and thermally driven voltage signals, then one should have

$$\frac{\Delta\rho_{xy}^{\phi,SMR}}{\Delta\rho_{xy}^{z,SMR}} = \frac{\Delta S_{xy}^{\phi,SMR}}{\Delta S_{xy}^{zSMR}} \quad (12)$$

when all coefficients are measured at the same temperature. In this case, it should also be possible to determine θ_{SN}/θ_{SH} by taking the ratio of either Eqs. (10) and (3) or Eqs. (11) and (4),

$$\frac{\theta_{SN}}{\theta_{SH}} = \frac{\Delta S_{xy}^{\phi,SMR}}{S_{HM}}\frac{\rho_0}{\Delta\rho_{xy}^{\phi,SMR}} = \frac{\Delta S_{xy}^{z,SMR}}{S_{HM}}\frac{\rho_0}{\Delta\rho_{xy}^{z,SMR}}. \quad (13)$$

In the case of an electrically conducting magnetic film, such as Pt magnetized by the MPE, magnetization-dependent deflection of electrons can also produce both electrically and thermally driven transverse voltage signals. In this case the longitudinal and transverse resistivities take the form [1]

$$\rho_{xx} = \rho_0 + \Delta\rho_{xy}^{\phi,AMR}m_x^2, \quad (14)$$

$$\rho_{xy} = \Delta\rho_{xy}^{z,AHE}m_z - \Delta\rho_{xy}^{\phi,AMR}m_xm_y, \quad (15)$$

where $\Delta\rho_{xy}^{\phi,AMR}$ is the coefficient of anisotropic magnetoresistance (AMR) and $\Delta\rho_{xy}^{z,AHE}$ is the coefficient of the anomalous Hall effect. The thermal analogue for the transverse voltage contains terms corresponding to the anomalous Nernst effect (ANE) and planar Nernst effect,

$$\frac{V_{xy}^{T-AMR}}{L_y} = -\left(\Delta S_{xy}^{z,ANE}m_z - \Delta S_{xy}^{\phi,PNE}m_xm_y\right)\nabla T_{ip}. \quad (16)$$

Within an electrically conducting magnet, in general, the equality analogous to Eq. (12) does not hold. For example, we show data for 1-nm-thick CoFeB samples in the Supplemental Material [17] for which $\Delta S_{xy}^{\phi,AMR}$ is very weak, below our detection limit, so $\Delta\rho_{xy}^{\phi,AMR}/\Delta\rho_{xy}^{z,AHE}$ is, at least, a factor of 20 greater than $\Delta S_{xy}^{\phi,PNE}/\Delta S_{xy}^{z,ANE}$. This difference can be understood based on Mott's relation [2] (see the Supplemental Material [17]).

III. Experimental methods. Experiments were performed on bilayers of TmIG with both W and Pt. The TmIG films (6 nm) were grown on single-crystal (111) gadolinium gallium garnet (GGG) substrates via pulsed laser deposition [18]. The TmIG has perpendicular magnetic anisotropy with an anisotropy field of 1.3 kOe (see the Supplemental Material [17]). After TmIG growth, the samples were transferred through air to a separate vacuum system where W (4 nm) or Pt (4 nm) was deposited by sputtering without further surface treatment. The average resistivities of the W and Pt films are 204 and 46 $\mu\Omega$ cm. The high resistivity in the W films indicates that they are primarily β phase [19]. Device structures were patterned by optical lithography and then Ar-ion milling fully through the TmIG to the GGG substrate so that the only TmIG remaining is within the TmIG/HM wire (see the Supplemental Material [17] for more details).
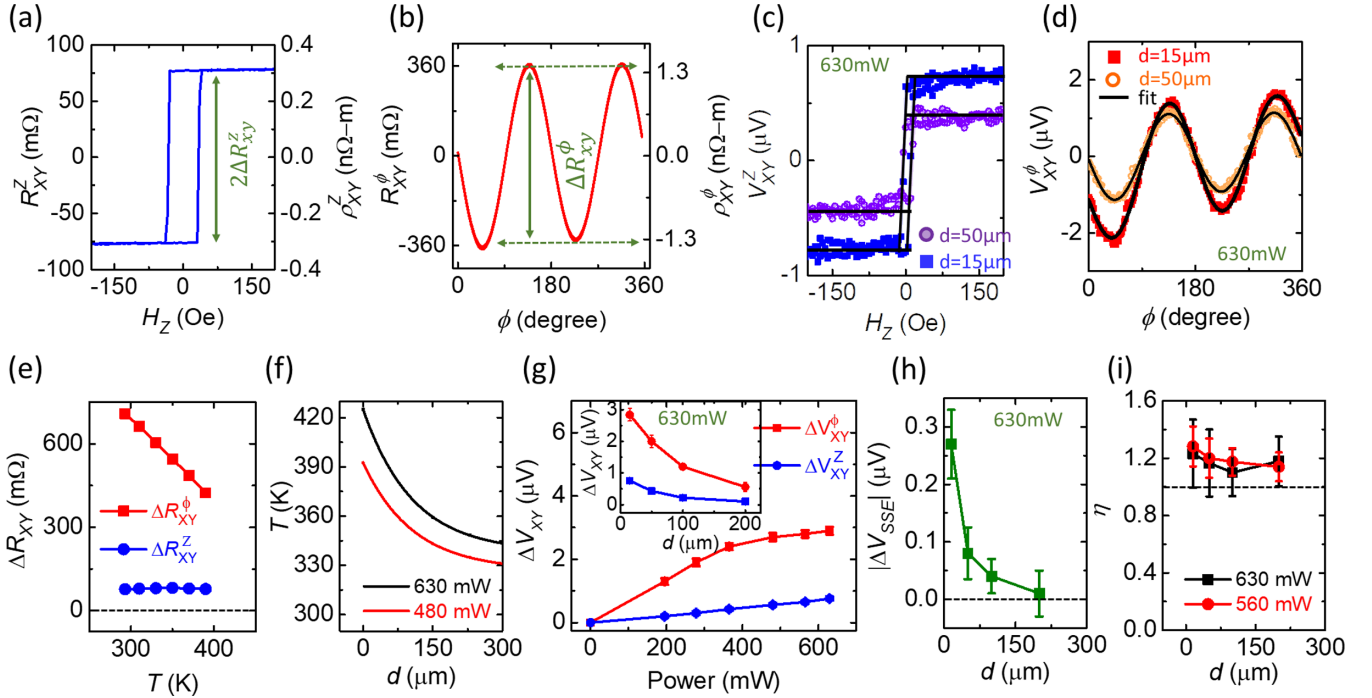
FIG. 2. Results for TmIG/W. Hall resistance of TmIG/W for (a) out-of-plane magnetic-field sweep and (b) in-plane field rotation for a field magnitude of 2.7 kOe. Thermally induced transverse voltages, (c) V_{xy}^z and (d) V_{xy}^ϕ, for a heater power of 630 mW and for two different heater spacings, $d = 15\,\mu$m (closed squares) and 50 μm (open circles). (e) Temperature dependence of ΔR_{xy}^ϕ (red) and ΔR_{xy}^Z (blue). (f) Temperature profile as function of d for heater power, $P_{\text{heater}} = 630$ mW (black) and 490 mW (red). (g) Heater power dependence of ΔV_{xy}^ϕ (red) and ΔV_{xy}^z (blue) for $d = 15\,\mu$m. Inset of (g): Dependence on d for ΔV_{xy}^ϕ (red) and ΔV_{xy}^z (blue) for $P_{\text{heater}} = 630$ mW. (h) Spin-Seebeck component ΔV_{SSE} as function of d for $P_{\text{heater}} = 630$ mW. (i) Variation of η as a function of d for $P_{\text{heater}} = 630$ mW (black) and 560 mW (red).

We measure ρ_{xx} for both TmIG/W [Fig. 1(d)] and TmIG/Pt [Fig. 1(e)] whereas rotating the H_{ext} (with magnitude 20 kOe, much higher than the anisotropy field) on the z-x and z-y planes [Fig. 1(b)]. Already we observe an important difference between the W and Pt samples. The TmIG/W devices show a large oscillation in ρ_{xx} for magnetic-field rotation on the y-z plane with an angular dependence that fits well $\propto m_y^2$, with negligible variation of ρ_{xx} for field rotation on the x-z plane. This is consistent with a signal entirely due to SMR [Eq. (1)] with negligible AMR [Eq. (14)]. In contrast, the TmIG/Pt sample has significant variation in ρ_{xx} for field rotations on both x-z and y-z planes, suggesting contributions from both SMR and AMR. Since TmIG is insulating, the presence of significant AMR in TmIG/Pt suggests the influence of a magnetic proximity effect in the Pt layer as has been reported previously [20,21].

To measure the transverse voltages produced by ∇T, we made TmIG/HM wires 650-μm long (L_y) and 20-μm wide (L_x) placed between two heater lines made of 15-nm thick and 200-μm wide Pt as shown in Fig. 1(c). The separation d between the TmIG/HM wires and each heater line was varied in different devices between 15 and 200 μm. We calibrated the temperature in the sample wires as a function of d by measuring the resistances of both the heater wire and the sample wires when current is flowing in the heater and comparing to independent measurements of resistance as a function of temperature using external heating of the sample chip. Based on these measurements we map ∇T_{ip} as a function of heater spacing [Fig. 2(f)] (Supplementary Information). We explored

heater temperatures up to 400 K, which is significantly less than the 550-K Curie temperature of the TmIG.

IV. Measurements of tranverse magnetoresistance and Nernst effect for TmIG/W. Our measurements of the E-driven Hall resistance for TmIG/W [Fig. 2(a) and 2(b)] as a function of magnetic-field angle fit well to the dependence,

$$R_{xy} = \Delta R_{xy}^z m_z + \Delta R_{xy}^\phi m_x m_y \qquad (17)$$

We determine ΔR_{xy}^z by sweeping H_{ext} perpendicular to the sample plane [e.g., Fig. 2(a)], and ΔR_{xy}^ϕ by rotating H_{ext} on the x-y plane [Fig. 2(b)]. We have measured ΔR_{xy}^Z and ΔR_{xy}^ϕ from room temperature to 390 K as shown with the blue and red curves in Fig. 2(e).

To measure the thermally driven transverse voltage [Figs. 2(c) and 2(d)], we apply current through one of the Pt heaters adjacent to the TmIG/W wire, which generates ∇T both in the sample plane ∇T_{ip}, and out of the plane, ∇T_{op} at the position of the TmIG/W wire [Fig. 1(a)]. We then measure the transverse voltage in the TmIG/W wires generated as a function of changing the direction of H_{ext} [Figs. 2(c) and 2(d)]. For a fixed heater power, we find that the transverse voltage as a function of magnetic-field angle is well described by

$$V_{xy}^T = \Delta V_{xy}^z m_z + \Delta V_{xy}^\phi m_x m_y + \Delta V_{\text{SSE}} m_x. \qquad (18)$$

We measure ΔV_{xy}^z by sweeping H_{ext} perpendicular to the sample plane [Fig. 2(c)]. ΔV_{xy}^ϕ and ΔV_{SSE} are determined using measurements as a function of rotating H_{ext} on the sample plane with a fit to the function $\Delta V_{xy}^\phi \sin\phi\cos\phi + \Delta V_{\text{SSE}}\cos\phi$
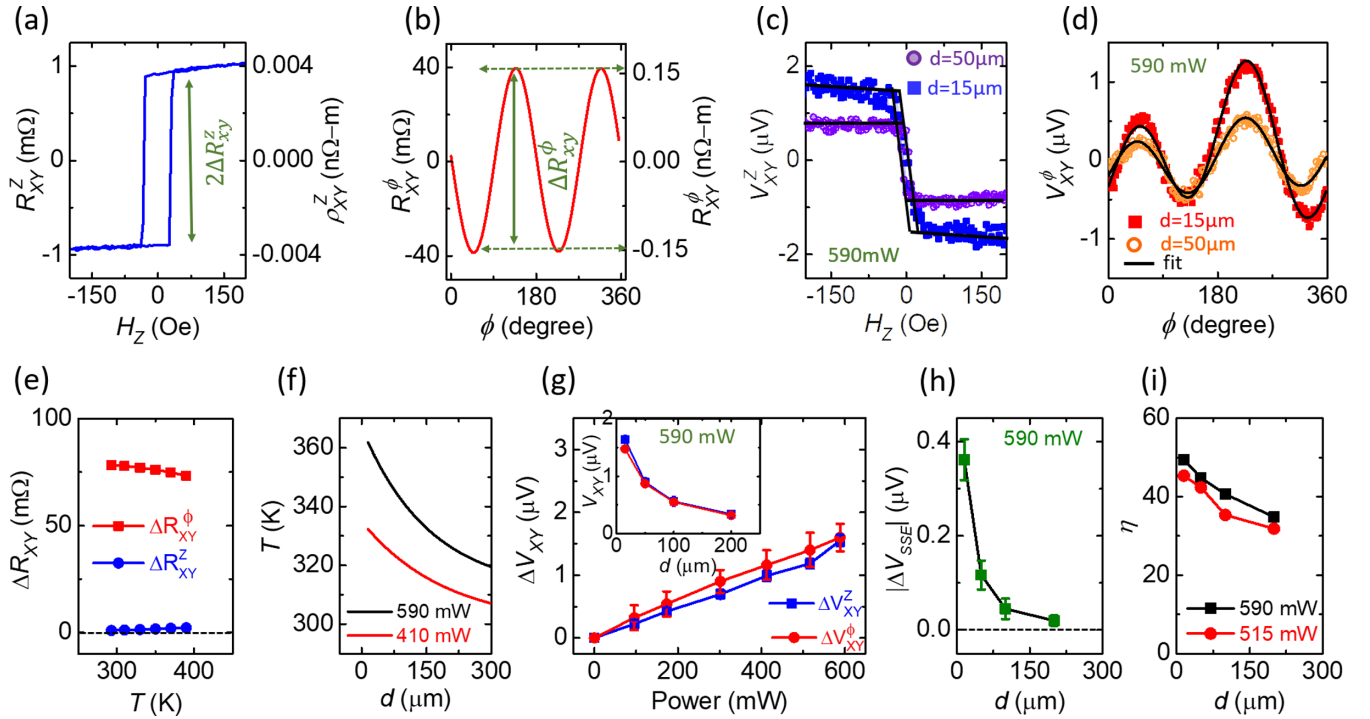
FIG. 3. Results for TmIG/Pt. Hall resistance of TmIG/Pt for (a) out-of-plane magnetic-field sweep and (b) in-plane field rotation for a field magnitude of 2.7 kOe. Thermally induced transverse voltages, (c) V_{xy}^z and (d) V_{xy}^ϕ, for a heater power of 590 mW and for two different heater spacings, $d = 15\,\mu$m (closed squares) and 50 μm (open circles). (e) Temperature dependence of ΔR_{xy}^ϕ (red) and ΔR_{xy}^Z (blue). (f) Temperature profile as function of d for heater power, $P_{\text{heater}} = 590$ mW (black) and 410 mW (red). (g) Heater power dependence of ΔV_{xy}^ϕ (red) and ΔV_{xy}^z (blue) for $d = 15\,\mu$m. Inset of (g): Dependence on d for ΔV_{xy}^ϕ (red) and ΔV_{xy}^z (blue) for $P_{\text{heater}} = 590$ mW. (h) Spin-Seebeck component ΔV_{SSE} as function of d for $P_{\text{heater}} = 590$ mW. (i) Variation of η as a function of d for $P_{\text{heater}} = 590$ mW (black) and 515 mW (red).

[Fig. 2(d)]. We ascribe the term proportional to $\cos\phi$ to the longitudinal spin Seebeck effect (SSE) [22] produced by ∇T_{op}, that generates a transverse voltage by the inverse ISHE. All three contributions, ΔV_{xy}^z, ΔV_{xy}^ϕ, and ΔV_{SSE}, decrease with increasing spacing between the heater and the TmIG/W wire [inset of Figs. 2(g) and 2(h)] as expected on account of the decreasing thermal gradients with the ΔV_{SSE} term (corresponding to ∇T_{op}) decreasing fastest [Fig. 2(h)] such that the contribution from ∇T_{op} becomes negligibly small for spacings greater than 100 μm in the range of heater power we explored.

To test whether the mechanism behind SMR is sufficient to explain both the electrically driven and thermally driven transverse voltages, we consider the ratio,

$$\eta = \left| \frac{\Delta R_{xy}^\phi / \Delta R_{xy}^z}{\Delta V_{xy}^\phi / \Delta V_{xy}^z} \right| = \left| \frac{\Delta \rho_{xy}^\phi / \Delta \rho_{xy}^z}{\Delta S_{xy}^\phi / \Delta S_{xy}^z} \right|. \quad (19)$$

As noted above [Eq. (12)] if SMR is the dominant spin-current detection mechanism contributing to both electrically driven and thermally driven signals, then η is predicted to be equal to 1. In making this comparison, it is important to take into account that during the thermally driven measurements the TmIG/W wires are heated substantially above room temperature [Fig. 2(g)], so we make the comparisons using values of ΔR_{xy}^ϕ and ΔR_{xy}^z at the same elevated temperatures present for the thermally driven measurements. The results are shown in Fig. 2(i). Over a range of heater spacing from 15 to 200 μm we find that ratio η is equal to one within 20%, which is on the

scale of the experimental uncertainty in the measured values. We conclude that SMR is the dominant spin-current detection mechanism in determining both the electrically driven and thermally driven signals in TmIG/W.

V. Measurements of tranverse magnetoresistance and Nernst effect for TmIG/Pt. Figure 3 shows results for the electrically driven and thermally driven transverse voltages for the TmIG/Pt samples analogous to those shown in Fig. 2 for TmIG/W. The signs of the electrically driven coefficients ΔR_{xy}^ϕ and ΔR_{xy}^z are the same for both heavy metals [compare Figs. 2(a) and 2(b) with Figs. 3(a) and 3(b)], but the signs of the thermally driven signals ΔV_{xy}^ϕ and ΔV_{xy}^z differ between TmIG/W and TmIG/Pt [compare Figs. 2(c) and 2(d) with Figs. 3(c) and 3d)]. There is also a striking difference on the scale of ΔR_{xy}^ϕ and ΔR_{xy}^z for TmIG/Pt [compare Figs. 2(e) and 3(e)]. The ratio $\Delta R_{xy}^\phi / \Delta R_{xy}^z$ varies from about 40 to 15 over the temperature range from room temperature to 400 K, whereas for TmIG/W this ratio varies only from about 4.6 to 2.5. Similar to TmIG/W, ΔV_{xy}^z, ΔV_{xy}^ϕ, and ΔV_{SSE} all decrease as a function of heater spacing d with ΔV_{SSE} decaying much faster [inset of Fig. 3(g) and 3(h)].

Using the same technique we employed for TmIG/W, we can test for TmIG/Pt whether the spin-current detection mechanism associated with SMR is sufficient to explain both the electrically driven and thermally driven transverse voltages by calculating the ratio η [Eq. (19)]. For TmIG/Pt we find $\eta = 30$–50 depending on the heater spacing d [Fig. 3(i)], which is substantially different from our result $\eta \approx 1$ for TmIG/W [Fig. 2(i)]. We, therefore, conclude for TmIG/Pt that the SMR

spin-current detection mechanism cannot be dominant in determining both the electrically driven and thermally driven transverse voltages in this system. Based on previous measurements of a magnetic proximity effect in TmIG/Pt bilayers at room temperature [20], and our observation of an AMR signal in the TmIG/Pt samples [Fig. 1(d)] consistent with a MPE in the Pt, we suggest that the difference between the TmIG/Pt and TmIG/W samples is the existence of an electrically conducting magnetic layer in the Pt due to the proximity effect at the measurement temperature. The influence of a MPE in TmIG/Pt but not TmIG/W in our measurements is consistent with previous measurements that the onset temperature of the MPE upon cooling in TmIG(6 nm)/Pt is well above room temperature whereas in TmIG(6 nm)/W it is well below room temperature [20].

Previously, Avci *et al.* studied similar TmIG/Pt samples and also found values for $\eta \approx 8$–10 [23], qualitatively similar to our result in that the value was much greater than 1. Instead of a MPE, they suggested that the mechanism for this result was a thermal spin-drag effect in which the SSE of TmIG due to ∇T_{op} induces spin accumulation in the heavy metal, and ∇T_{ip} then induces an in-plane spin current that generates a transverse voltage due to the inverse SHE. We can rule out this possibility for our samples because the dependence of our signals (ΔV_{xy}^z) on heater power [Figs. 2(g) and 3(g)] is to a good approximation linear, whereas $\nabla T_{op} \nabla T_{ip} \propto (\text{heaterpower})^2$.

VI. Discussion. Since we have determined that SMR is the dominant readout mechanism for both electrically driven and thermally driven signals in TmIG/W (but not TmIG/Pt), our data allow us to consider the mechanism by which the thermally induced spin currents are generated in TmIG/W by analyzing the value of θ_{SN} [Eqs. (5) and (7)].

If the transverse spin current generation in W was due entirely to the intrinsic SHE [3,24], theory predicts that one should be able to compute the transverse spin current as an appropriate integral over occupied electronic states of a transverse anomalous velocity,

$$\vec{v}(\vec{k}, \vec{\sigma}) = e\vec{E} \times \tilde{\Omega}(\vec{k}, \vec{\sigma}), \tag{20}$$

where $\vec{k}$ is the electron wave-vector, $\vec{\sigma}$ is a spin index, $\tilde{\Omega}(\vec{k}, \vec{\sigma})$ is the spin Berry curvature (see Ref. [25] for an elementary discussion). Equation (20) implies that even in the absence of any net J_C, a ∇T that gives rise to an electric field due to the Seebeck effect should generate the same spin current as if the electric field were applied externally. In other words, under the assumptions associated with Eq. (20), θ_{SN}^0 in Eq. (6) should be zero and, hence, one should have $\theta_{SN} = -\theta_{SH}$ by Eq. (7).

Making a precise measurement of S_{HM} for use in Eq. (5) of materials at room temperature is nontrivial because it is not possible to use a superconductor as a reference electrode. We have performed measurements on our TmIG (6 nm)/W

(4 nm) films using Au wires as reference electrodes and have corrected for the literature value of the absolute Seebeck coefficient of Au, $\sim +1.5 \mu$V/K [26] (see Supplemental Material [17]). The resulting estimate for the Seebeck coefficient for our 4-nm W films is $S_{HM}(W) = -4.5 \pm 0.5 \mu$V/K. With this value, Eq. (13) yields $\theta_{SN}/\theta_{SH} = -1.9 \pm 0.6$ based on $\frac{\Delta S_{xy}^{\phi,\text{SMR}}}{S_{HM}} \frac{\rho_0}{\Delta \rho_{xy}^{\phi,\text{SMR}}}$ and $\theta_{SN}/\theta_{SH} = -2.4 \pm 0.6$ based on $\frac{\Delta S_{xy}^{z,\text{SMR}}}{S_{HM}} \frac{\rho_0}{\Delta \rho_{xy}^{z,\text{SMR}}}$. These values are consistent with previous reports for bilayers consisting of W with a conducting magnet [12,13]. The fact that θ_{SN}/θ_{SH} is of order -1 suggests that the intrinsic SHE largely sets the scale of the thermally generated J_S in W. This is interesting in that even in the absence of any net charge current flow spin current is still driven by an electric field. However, we suggest that this is not the whole story, since θ_{SN}/θ_{SH} differs from -1 by more than our estimated experimental uncertainty. Deviations might result from extrinsic contributions to the SHE or strong energy dependence of the spin Hall ratio.

VII. Summary. In conclusion, we find that the mechanisms that lead to the generation of transverse voltages are different between TmIG/W and TmIG/Pt samples. In TmIG/W, both electrically generated and thermally generated transverse voltages are consistent with the spin-current detection mechanism associated with SMR. For TmIG/Pt, in contrast, the ratio of the thermally generated anomalous Nernst signal ΔS_{xy}^z to the corresponding anomalous Hall signal $\Delta \rho_{xy}^z$ is much larger than would be expected for a purely SMR-based spin-current detection mechanism. We suggest the reason for this difference is that proximity-induced magnetism exists near the TmIG/Pt interface in an electrically conducting interface layer at room temperature, allowing for an anomalous Hall signal in addition to signals due to SMR.

[1] N. Nagaosa, J. Sinova, S. Onoda, A. H. MacDonald, and N. P. Ong, Anomalous hall effect, Rev. Mod. Phys. **82**, 1539 (2010).

[2] Y. Pu, D. Chiba, F. Matsukura, H. Ohno, and J. Shi, Mott Relation for Anomalous Hall and Nernst Effects in Ga$_{1-x}$Mn$_x$ As

Ferromagnetic Semiconductors, Phys. Rev. Lett. **101**, 117208 (2008).

[3] J. Sinova, S. O. Valenzuela, J. Wunderlich, C. H. Back, and T. Jungwirth, Spin hall effects, Rev. Mod. Phys. **87**, 1213 (2015).

[4] A. Bose and A. A. Tulapurkar, Recent advances in the spin nernst effect, J. Magn. Magn. Mater. **491**, 165526 (2019).

[5] H. Nakayama, M. Althammer, Y.-T. Chen, K. Uchida, Y. Kajiwara, D. Kikuchi, T. Ohtani, S. Geprägs, M. Opel, S. Takahashi, R. Gross, G. E. W. Bauer, S. T. B. Goennenwein, and E. Saitoh, Spin Hall Magnetoresistance Induced by a Nonequilibrium Proximity Effect, Phys. Rev. Lett. **110**, 206601 (2013).

[6] M. Althammer, S. Meyer, H. Nakayama, M. Schreier, S. Altmannshofer, M. Weiler, H. Huebl, S. Geprägs, M. Opel, R. Gross, D. Meier, C. Klewe, T. Kuschel, J.-M. Schmalhorst, G. Reiss, L. Shen, A. Gupta, Y.-T. Chen, G. E. W. Bauer, E. Saitoh, and S. T. B. Goennenwein, Quantitative study of the spin hall magnetoresistance in ferromagnetic insulator/normal metal hybrids, Phys. Rev. B **87**, 224401 (2013).

[7] S. Y. Huang, X. Fan, D. Qu, Y. P. Chen, W. G. Wang, J. Wu, T. Y. Chen, J. Q. Xiao, and C. L. Chien, Transport Magnetic Proximity Effects in Platinum, Phys. Rev. Lett. **109**, 107204 (2012).

[8] B. F. Miao, S. Y. Huang, D. Qu, and C. L. Chien, Physical Origins of the New Magnetoresistance in Pt/Yig, Phys. Rev. Lett. **112**, 236601 (2014).

[9] B. F. Miao, L. Sun, D. Wu, C. L. Chien, and H. F. Ding, Tuning the magnetoresistance symmetry of Pt on magnetic insulators with temperature and magnetic doping, Appl. Phys. Lett. **110**, 222402 (2017).

[10] Y.-T. Chen, S. Takahashi, H. Nakayama, M. Althammer, S. T. B. Goennenwein, E. Saitoh, and G. E. W. Bauer, Theory of spin hall magnetoresistance, Phys. Rev. B **87**, 144411 (2013).

[11] S. Meyer, Y.-T. Chen, S. Wimmer, M. Althammer, T. Wimmer, R. Schlitz, S. Geprägs, H. Huebl, D. Ködderitzsch, H. Ebert, G. E. W. Bauer, R. Gross, and S. T. B. Goennenwein, Observation of the spin nernst effect, Nature Mater. **16**, 977 (2017).

[12] P. Sheng, Y. Sakuraba, Y.-C. Lau, S. Takahashi, S. Mitani, and M. Hayashi, The spin nernst effect in tungsten, Sci. Adv. **3**, e1701503 (2017).

[13] D. J. Kim, C. Y. Jeon, J. G. Choi, J. W. Lee, S. Surabhi, J. R. Jeong, K. J. Lee, and B. G. Park, Observation of transverse spin nernst magnetoresistance induced by thermal spin current in ferromagnet/non-magnet bilayers, Nat. Commun. **8**, 1400 (2017).

[14] A. Bose, S. Bhuktare, H. Singh, S. Dutta, V. G. Achanta, and A. A. Tulapurkar, Direct Detection of Spin Nernst Effect in Platinum, Appl. Phys. Lett. **112**, 162401 (2018).

[15] A. Bose, A. S. Shukla, S. Dutta, S. Bhuktare, H. Singh, and A. A. Tulapurkar, Control of magnetization dynamics torque, Phys. Rev. B **98**, 184412 (2018).

[16] J.-M. Kim, D.-J. Kim, C.-Y. Cheon, K.-W. Moon, C. Kim, P. Cao Van, J.-R. Jeong, C. Hwang, K.-J. Lee, and B.-G. Park, Observation of thermal spin–orbit torque in w/cofeb/mgo structures, Nano Lett. **20**, 7803 (2020).

[17] Supplemental Material at http://link.aps.org/supplemental/10.1103/PhysRevB.105.L100408 for the details of the sample prepration, temperature calibration, Seebeck coefficient calculation and the additional experimental data along with the derivation from Mott' relation.

[18] A. Quindeau, C. O. Avci, W. Liu, C. Sun, M. Mann, A. S. Tang, M. C. Onbasli, D. Bono, P. M. Voyles, Y. Xu, J. Robinson, G. S. D. Beach, and C. A. Ross, $Tm_3Fe_5O_{12}$/Pt Heterostructures with perpendicular magnetic anisotropy for spintronic applications, Adv. Electron. Mater. **3**, 1600376 (2017).

[19] C.-F. Pai, L. Liu, Y. Li, H. W. Tseng, D. C. Ralph, and R. A. Buhrman, Spin Transfer Torque Devices Utilizing the Giant Spin Hall Effect of Tungsten, Appl. Phys. Lett. **101**, 122404 (2012).

[20] Q. Shao, A. Grutter, Y. Liu, G. Yu, C.-Y. Yang, D. A. Gilbert, E. Arenholz, P. Shafer, X. Che, C. Tang, M. Aldosary, A. Navabi, Q. L. He, B. J. Kirby, J. Shi, and K. L. Wang, Exploring interfacial exchange coupling and sublattice effect in heavy metal/ferrimagnetic insulator heterostructures using hall measurements, x-ray magnetic circular dichroism, and neutron reflectometry, Phys. Rev. B **99**, 104401 (2019).

[21] J. J. Bauer, P. Quarterman, A. J. Grutter, B. Khurana, S. Kundu, K. A. Mkhoyan, J. A. Borchers, and C. A. Ross, Magnetic proximity effect in magnetic-insulator/heavy-metal heterostructures across the compensation temperature, Phys. Rev. B **104**, 094403 (2021).

[22] K. I. Uchida, H. Adachi, T. Ota, H. Nakayama, S. Maekawa, and E. Saitoh, Observation of Longitudinal Spin-Seebeck Effect in Magnetic Insulators, Appl. Phys. Lett. **97**, 172505 (2010).

[23] C. O. Avci, E. Rosenberg, M. Huang, J. Bauer, C. A. Ross, and G. S. D. Beach, Nonlocal Detection of Out-of-Plane Magnetization in a Magnetic Insulator by Thermal Spin Drag, Phys. Rev. Lett. **124**, 027701 (2020).

[24] G. Vignale, Ten years of spin hall effect, J. Supercond. Nov. Magn. **23**, 3 (2010).

[25] D. C. Ralph, BerryCurvature, Semiclassical electron dynamics, and topological materials: Lecture notes for introduction to solid state physics, arXiv:2001.04797.

[26] N. Cusack and P. Kendall, The absolute scale of thermoelectric power at high temperature, Proc. Phys. Soc. **72**, 898 (1958).